Research Article

Magnetite Nanoparticles–Antibiotic Composites Boost Antibacterial Efficacy Against Multidrug-Resistant Bacteria

Sereen M.B. Bataineh[1*], Samya M. Abu-Zreg[1], Isam M. Arafa[2], Hanan M. Hammouri[3] and Homa Darmani[1]

[1]Department of Biotechnology and Genetic Engineering, Faculty of Science and Arts, Jordan University of Science and Technology, P.O. Box 3030, Irbid 22110, Jordan; [2]Department of Applied Chemistry, Faculty of Science and Arts, Jordan University of Science and Technology, P.O. Box 3030, Irbid 22110, Jordan; [3]Department of Mathematics and Statistics, Faculty of Science and Arts, Jordan University of Science and Technology, P.O. Box 3030, Irbid 22110, Jordan.

Abstract | Many early-generation antibiotics, previously deemed ineffective due to bacterial resistance. This study aimed to reconsider the potential use of antibiotics to treat bacterial infections through their integration with metal oxide nanoparticles (MONPs), which have shown promise in delaying the growing crisis of resistance to the commonly used antibiotics. Magnetite nanoparticles (MagNPs)–antibiotic composites were prepared and characterized using Fourier transform infrared spectroscopy (FT-IR) to confirm proper conjugation and their antibacterial effects were evaluated. The antibacterial activity of MagNP–antibiotic composites was evaluated against both susceptible and resistant strains of *Staphylococcus aureus* and *Escherichia coli via* the microdilution method to determine their minimal inhibitory concentration (MIC) after 21 h of incubation. Scanning electron microscopy (SEM) analysis showed that the NPs had a spherical morphology, while X-ray diffraction (XRD) analysis estimated the crystallite sizes that ranged from 13 to 21 nm. Fourier transform infrared (FT-IR) spectroscopy revealed the existence of intermolecular interactions between the antibiotics and MagNPs. An enhanced antibacterial effect was observed, as indicated by a remarkable reduction in the MIC values for all the MagNP–antibiotic composites against *S. aureus* and susceptible *E. coli*. In contrast, an activity against the MDR *E. coli* BAA 2452 was observed with MagNPs–ampicillin (MagNPs–Amp), MagNPs–chloramphenicol (MagNPs–Chl), and MagNPs–ciprofloxacin (MagNPs–Cip) composites. The MagNP–antibiotic composites demonstrated enhanced antibacterial activity, particularly against multi-drug resistant (MDR) strains. The MIC values for the MRSA strain were reduced by 8-fold (MagNPs-Amp and MagNPs-Chl) and nearly 12-fold (MagNP-Cip). Most remarkably, the MagNPs-Cip composite achieved up to a 60-fold MIC reduction against MDR *E. coli* BAA 2452, while the MagNPs-Amp composite critically restored susceptibility in a previously unaffected MDR *E. coli* strain. These findings strongly suggest that this MagNPs–antibiotic composite effectively evades the existing resistance mechanisms, suggesting additional optimization for wider antibacterial potentials.

Received | April 29, 2026; **Revised** | June 25, 2026; **Accepted** | July 04, 2026; **Published** | July 13, 2026
***Correspondence** | Sereen M.B. Bataineh, Department of Biotechnology and Genetic Engineering, Faculty of Science and Arts, Jordan University of Science and Technology, P.O. Box 3030, Irbid 22110, Jordan; **Email:** smbataineh3@just.edu.jo
Citation | Bataineh, S.M.B., S.M. Abu-Zreg, I.M. Arafa, H.M. Hammouri and H. Darmani. 2026. Magnetite nanoparticles–antibiotic composites boost antibacterial efficacy against multidrug-resistant bacteria. *Novel Research in Microbiology Journal,* 10(4): 377-395.
DOI | https://dx.doi.org/10.17582/journal.nrmj/2026.10.4.377.395
Keywords | Antibiotics, *Escherichia coli*, Magnetite nanoparticles, *Staphylococcus aurues*, Synergistic antibacterial efficacy

Introduction

Antibiotic resistance has emerged as a significant health concern, undermining the effectiveness of traditional treatments. They impede bacterial growth or reproduction through various mechanisms (Uddin *et al.*, 2021; Theodorakis *et al.*, 2024), such as disrupting the cell wall or interfering with the synthesis of critical enzymes, proteins, or nucleic acids (RNA and DNA) (Uddin *et al.*, 2021). Despite their use for treating infections (Wang *et al.*, 2022), their overuse and misuse have led to the development of multi-drug-resistant (MDR) bacterial strains. These strains can acquire and disseminate resistance genes (Walsh *et al.*, 2023), rendering many existing antibiotics ineffective and complicating the treatment of bacterial infections (Uddin *et al.*, 2021; Cook and Wright, 2022; Wang *et al.*, 2022; Corona *et al.*, 2023; Walsh *et al.*, 2023; Grooters *et al.*, 2024; Theodorakis *et al.*, 2024). Making matters worse is the limited progress in introducing new antibiotic therapies (Uddin *et al.*, 2021). *Staphylococcus aureus* and *Escerichia coli*, in particular, are major pathogens that cause nosocomial infections, with their rising resistance to traditional antibiotics, representing a major health threat (Uddin *et al.*, 2021). Consequently, alternative strategies are urgently needed to mitigate the limitations of the current antibiotics and limit the spread of resistance genes (Mouton, 1999; Worthington and Melander, 2013; Khezerlou *et al.*, 2018; Zhu *et al.*, 2021; Ahmed *et al.*, 2023).

On the other hand, nanoparticles (NPs) have emerged as promising materials for developing novel antibacterial agents (Ezealigo *et al.*, 2021). Due to their advantageous properties such as small size (< 100 nm), large surface area, and inherent antibacterial activity, NPs can disrupt bacterial cell wall synthesis, inhibit biofilm formation, and weaken bacterial cells, making them more susceptible to antibiotics (Xu *et al.*, 2019; Abo-Zeid and Williams, 2020). Moreover, many NPs can generate reactive oxygen species (ROS), which may damage bacterial membranes, proteins, and genetic material, ultimately resulting in cell death (Xu *et al.*, 2019; Abo-Zeid and Williams, 2020; Ezealigo *et al.*, 2021).

For instance, silver NPs (AgNPs) can inhibit the growth of *E. coli* and yeast (Kim *et al.*, 2007). However, their use is constrained due to their *in vivo* toxic effects on cultured human cells (Soto *et al.*, 2007) and several environmental concerns, particularly their risk of impairing the nitrifying bacteria in soil, thereby affecting nitrogen availability for plant growth (Zheng *et al.*, 2017). Similarly, titanium dioxide NPs (TiO_2NPs) exhibit notable antibacterial and antitumor activity, due to their photosensitizing and photodynamic properties (Dizaj *et al.*, 2014; Joseph, 2023), and are already employed in bone and dental implants (Nikolova and Chavali, 2020). However, prolonged exposure raises toxicity concerns (Shi *et al.*, 2013).

In this context, magnetic iron oxide NPs (MagNPs) offer a strategic and safer option for combating bacterial infections and other medical applications due to their unique physicochemical properties (Ezealigo *et al.*, 2021; Zhang and Miao, 2024). These include their nanoscale dimensions, which give them a high surface area-to-volume ratio that allows them to obstruct pathogens and superparamagnetic behavior, facilitating their orientation *via* external magnets for tumor therapy, drug delivery, and magnetic hyperthermia (Xu *et al.*, 2019; Ezealigo *et al.*, 2021). Their biocompatibility and biodistribution in the body make them safe as a MRI contrast agent (Zhang and Miao, 2024). In addition, they are harmless, exhibiting low toxicity and side effects in the human body (Ezealigo *et al.*, 2021; Shoudho *et al.*, 2024; Zhang and Miao, 2024; Hosseinzadeh, 2025). These NPs can be used alone or in combination with other materials to suppress the resistant pathogens. Their magnetic properties enable targeted delivery systems to infected organs or tissues and assist in infection imaging, detection, and separation (Xu *et al.*, 2019). This therapeutic approach may help overcome resistance, reduce antibiotic dosage requirements, and limit the development and spread of further antibiotic resistance (Abo-Zeid and Williams, 2020).

Mouton *et al.* suggested that using two or more antibiotics can help prevent bacteria from developing resistance (Mouton, 1999). This approach works by targeting bacteria with multiple agents simultaneously, making it harder for them to evade treatment and disrupt their ability to maintain resistance mechanisms (Mouton, 1999). As a result, this combination approach has sparked extensive research into a variety of alternatives to combat antibiotic-resistant bacteria (Wang *et al.*, 2022). These include using multiple antibiotics as well as combining them with natural products, plant extracts, or nanomaterials (Wang *et al.*, 2022).

To develop these combinations, several techniques have been employed, such as checkerboard assays (Yap *et al*., 2013), conjugation (Armijo *et al*., 2020), various synthesis procedures (Murei *et al*., 2020), direct mixing (Current *et al*., 2017), and other innovative methods (Rashid *et al*., 2021; Wehbe *et al*., 2024). For example, Yap *et al*. studied combinations of commercial plant essential oils and different β-lactam antibiotics against various strains of *E. coli* using the checkerboard assay (Yap *et al*., 2013). On the other hand, other combinations have been developed for elimination of the antibiotic pollutants in the environment (Han *et al*., 2025). A photocatalyst was synthesized from nanodiamond/TiO_2 (Oueslati *et al*., 2024) and two-dimensional transition metal carbide/nitride (MXene) to boost the degradation of tetracycline in water. Thus, the combined materials achieve synergistic benefits at both the medical and environmental levels (Oueslati *et al*., 2024; Han *et al*., 2025). Similarly, Bhattacharya and Neogi (2017) successfully conjugated gentamicin with FeONPs, demonstrating bactericidal activity against *S. aureus*, *E. coli*, *Pseudomonas aeruginosa*, and *Bacillus subtilis* (Bhattacharya and Neogi (2017). Murei *et al*. (2020) also reported the antibacterial efficacy of combining antibiotics (vancomycin, ampicillin, and penicillin) with *Pyrenacantha grandiflora* extracts and AgNPs for use against *Klebsiella pneumonia*, *E. coli*, and *S. aureus* (Murei *et al*., 2020). These results highlight the potential of repurposing the antibiotics to combat the resistant strains more effectively.

The present study aimed to enhance the bactericidal efficacy of older-generation antibiotics to combat resistance and restore their clinical efficacy. This study introduced a novel composite achieved by preparing MagNPs–antibiotic composites through a 21-h mixing process conducted at room temperature with continuous shaking. The MagNPs were selected due to their unique and advantageous characteristics, including low cytotoxicity and excellent biocompatibility. They also exhibit ferrimagnetic properties at room temperature and demonstrate high colloidal stability. Additionally, they are cost-effective and their antibacterial potential is well documented (Saqib *et al*., 2018).

Materials and Methods

Reagents

All chemicals and solvents were of analytical grade and used as received from the suppliers. $FeCl_3.6H_2O$ and $FeCl_2.4H_2O$ were purchased from Riedel-de Haën AG (Sleeze, Germany). We also utilized ammonium hydroxide 25% (Thermo Fisher Scientific, Hampton, NH, USA), absolute ethanol (AR grade, VWR chemicals, Randor, PA, USA), absolute methanol (Iso Lab Chemicals, Wertheim, Germany), Müller Hinton Agar (MHA) and broth (Oxoid Limited, Basingstoke, UK, Thermo Fisher Scientific USA), iodonitrotetrazolium chloride (INT) 98% (Acros Organics, Thermo Fisher Scientific, Hampton, NH, USA), normal saline ((NS, 0.9 % w/v sodium chloride, pharmaceutical solutions industry, Jaddah, Saudi Arabia), Ciprofloxacin ≥ 98% (Sigma-Aldrich, Co., Spruce Street, St. Louis, USA), Chloramphenicol (> 97%) (Bio Basic, Canada, Inc.), Ampicillin 95% (Combi-Blocks, San Diego, USA), and Cefoxitin 98% (CAYMAN Chemical company, Ann Arbor, Michigan, USA).

Magnetite nanoparticles synthesis

Magnetic iron oxide NPs (magnetite, Fe_3O_4, and NPs) were synthesized *via* a precipitation method using 1:2 molar ratio of ferrous chloride tetrahydrate ($FeCl_2.4H_2O$) and ferric chloride hexahydrate ($FeCl_3.6H_2O$) and dissolved in 100 ml deionized water under basic conditions, by adding 8 ml ammonia solution (25%) (Karaagac *et al*., 2011; Alomari *et al*., 2015; Al-Shabib *et al*., 2018) with sonication. The resulting mixture was filtered using a sterile Whatman qualitative filter paper (grade 1, no. 1001-150), washed thoroughly with sterile deionized distilled water, followed by absolute ethanol (3-5 times), and left overnight. The samples were dried in an oven at 80 ˚C for 2 d to yield dry black magnetic Fe_3O_4 NPs (Bataineh *et al*., 2024).

Physicochemical characterization

The physicochemical and topographical characteristics of MagNPs were assessed by various analytical techniques. Scanning electron microscopy (SEM) was utilized to examine the size, shape, surface morphology, and distribution of the NPs (Alomari *et al*., 2015; Bataineh *et al*., 2024). The SEM images were obtained using a Field Emission Scanning Electron Microscope Quanta FEG450, FEI Company, USA. X-ray diffraction (XRD) was used to analyze the crystal structure and calculate the average crystallite size of the NPs using Bragg's Law and the Scherrer equation (Alomari *et al*., 2015).

Moreover, the NPs' crystallite size (D) was estimated from the peak broadening of the two most intense diffraction peaks due to 311 and 440 planes using the Scherrer Equation 1, where κ, the shape factor for cubic-shaped crystals was 0.95; λ represent the wavelength of the X-ray beam (Cu = 0.1548 nm); β = the full width at the half maximum (FWHM) in radians; and θ was the Bragg angle.

$$D = \frac{\kappa\lambda}{\beta \cos\theta} \quad \ldots(1)$$

The XRD analysis was performed using an X-ray diffractometer from Rigaku (40 kV/40 mA X-ray scanning continuously 3-degree/min, ranging from 15 to 90 degrees using Kβ filter). Furthermore, the DLS analysis of MagNs, including the hydrodynamic diameter and zeta potential (ZP) were discussed in our previous publication (Bataineh *et al.*, 2024). Additionally, Fourier transform infrared spectroscopy (FT-IR) was conducted to identify the functional groups present on the surface of the synthesized MagNPs, both in their native forms and after combination with the selected antibiotics. The FT-IR spectra of the powdered samples of the MagNPs, along with the individual antibiotics, *i.e.*, ampicillin, cefoxitin, chloramphenicol, and ciprofloxacin were measured (Sahoo *et al.*, 2011; Ahire and Dicks, 2016; Sterren *et al.*, 2017; Chavan *et al.*, 2020). The FT-IR spectra were recorded in the range of 4000-400 cm^{-1} at room temperature using Bruker Vertex 70. XRD and FT-IR were plotted using OriginPro 2025b software (OriginLab Corporation, Northampton, MA, USA). The composites were prepared by co-mixing the synthesized MagNPs with the four antibiotics (Amp, Chl, Cip, and Cef) for 24 h at room temperature.

Microbiological assays

Strain metadata: The bacterial strains selected as representatives for Gram-positive and Gram-negative bacteria were as follows: *Staphylococcus aureus* ATCC 29213 [Methicillin-Sensitive (MSSA)], *Staph. aureus* ATCC 43300 [Methicillin-Resistant (MRSA)], *Escherichia coli* ATCC 25922 (wild type), and *E. coli* BAA 2452 [multi-drug-resistant, (MDR). All strains were provided by the Department of Basic Veterinary Medical Sciences, Faculty of Veterinary Medicine, Jordan University of Science and Technology (JUST), Jordan. The strains were preserved in 10% glycerol in Mueller–Hinton broth (MHB) at -80 °C and revived by culturing on Mueller–Hinton Agar (MHA) at 37 °C for 24 h before conducting the various assays.

Inoculum preperation

Fresh bacterial strains were cultivated on MHA and incubated overnight at 37°C. Single colony was transferred into 2 ml of MHB and incubated for 2 h (37). The turbidity of the inoculum was measured at 600 nm using a BioMate 3 UV-Vis spectrophotometer (Thermo Spectronic, USA), adjusted with sterile MHB to achieve an optical density of 0.08-0.13 (equivalent to 0.5 McFarland standards). The suspension was diluted ten-fold immediately before being loaded into the 96-well plate.

Conjugation of MagNP and antibiotics

Ampicillin (Amp), ciprofloxacin (Cip), cefoxitin (Cef), and chloramphenicol (Chl) were each prepared as stock solutions according to the manufacturers' instructions, in addition to the Clinical Laboratory Standards Institute guidelines (CLSI, 2020). Each antibiotic was dissolved in an appropriate solution: Amp was dissolved in 0.1 M phosphate buffer, pH 8, and diluted in 0.1 M phosphate buffer, pH 6; Cip dissolved and diluted in sterile distilled water; Cefoxitin (Cef) dissolved and diluted in sterile distilled water; and Chloramphenicol (Chl) dissolved in 95% ethanol and diluted in sterile distilled water. The prepared concentration was determined as the manufacturer's purity (ESCMID, 2003) and filtered using a 0.22-µm-pore filter. Aliquots of each antibiotic were stored at -20 °C until use (CLSI, 2020). The bactericidal activity of the combined MagNP–antibiotic formulations was assessed using the minimal inhibitory concentration (MIC) and minimal bactericidal concentration (MBC). Antibacterial assays were conducted individually for each antibiotic, MagNP alone, and their combination. Starting concentrations of 256 mg/ml for the NPs and 256 µg/ml for all antibiotics were used to obtain the MIC values for each agent against each tested strain according to CLSI protocols. For the combination assay, antibiotics at 2 ×MIC were mixed with MagNP at a concentration of 128 mg/ml and incubated for 21 h (Current *et al.*, 2017; Murei *et al.*, 2020; Bataineh *et al.*, 2024). The MagNP concentration used in the composites was fixed in all assays to ensure a consistent dose; however, the antibiotic concentrations were variable.

Determination of minimal inhibitory concentration (MIC) and minimal bactericidal concentration (MBC)

The MIC and MBC were used to assess the antibacterial activity of the MagNPs–antibiotic

composites against the tested bacterial strains. The microdilution method was used to determine the MIC, as described in CLSI guidelines (Bataineh *et al.*, 2024). Briefly, 100 µl of MHB was first dispensed into each well of a 96-well plate; 100 µl of the tested composites were added into the first well, followed by two-fold serial dilutions across 10 wells, and the final 100 µl were discarded.

Each well thus contained 100 µl of the test mixture strain (Bataineh *et al.*, 2024; Murei *et al.*, 2020), to which a standardized bacterial inoculum of 5×10^{-5} CFU/ml was added. Growth control wells contained MHB with bacterial inoculum only, while the negative control wells contained MHB only. The plates were incubated for 19 h at 37 °C. Afterward, 40 µl of 0.2% INT were added to each well and incubated for another hour. The MIC value was defined visually as the lowest concentration that completely inhibited the bacterial growth, indicated by the absence of a red/pink color change in the well (Bataineh *et al.*, 2024). The MBC test was conducted according to the established protocols (Bataineh *et al.*, 2024). Aliquots (10 µl) from the MIC, 2MIC, and 4MIC wells in addition to the growth control and negative control were subcultured into 90 µl fresh MHB in a new 96-well plate, followed by 10-fold serial dilutions. From each dilution, 10 µl were plated onto MHA plates and incubated for 19 h at 37 °C. The MBC was defined as the lowest concentration of the antibacterial agent that resulted in the development of less than 5 colonies on the subcultured MHA plates (Abu-Dalo *et al.*, 2019). All experiments were performed in triplicate in the same day. Additionally, a parallel set of experiments were conducted in triplicate using the same composites with only one hour of mixing incubation to compare the effectiveness of the different exposure times (Bataineh *et al.*, 2024).

Statistical analysis

Minimum inhibitory concentration values are presented as means (± SD) based on nine replicate. The JMP program version 17.0 from SAS Institute Inc. (Cary, NC, USA, 2022) was utilized to analyze the data. A Q-Q plot test showed that the data were not normally distributed. Therefore, the nonparametric Kruskal–Wallis test and the Wilcoxon rank test were employed to compare the MIC values of each antibiotic individually and in combination with MagNPs. Additionally, the Wilcoxon rank test was employed to compare the MIC values of the MagNP alone versus those combined with the antibiotics against the *Staph. aureus* strains. However, these tests were not performed for the *E. coli* strains that didn't display susceptibility to MagNPs alone, as their baseline MIC values were beyond the quantifiable limits of the assay. A p-value of ≤ 0.05 was considered significant.

Results

Magnetite NPs physicochemical characterization

The synthesized MagNPs were characterized using three physical techniques: SEM, XRD, and FT-IR. SEM was performed using a Quanta FEG microscope to assess the shape and size of the synthesized MagNPs under different magnifications ranging from 100 µm to 100 nm. The SEM images revealed that the MagNPs were uniformly spherical in shape with an estimated size below 60 nm and an average diameter of approximately 20 nm, as shown in Figure 1.

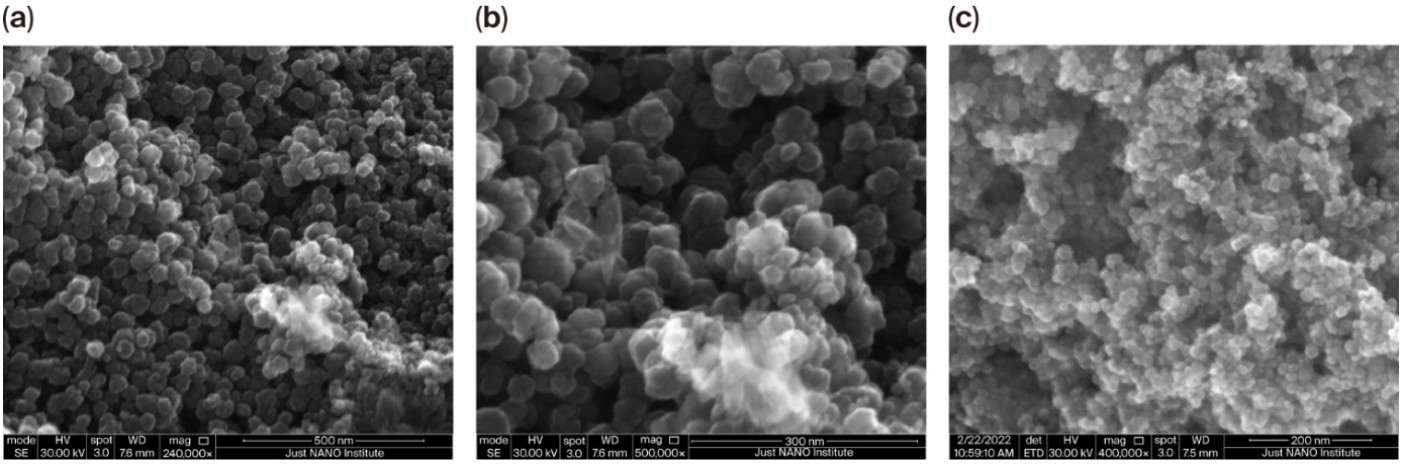

Figure 1: *Scanning electron microscopy* **(***SEM) images at a) 500 nm, b) 300 nm, and c) 200 nm for the synthesized MagNPs.*

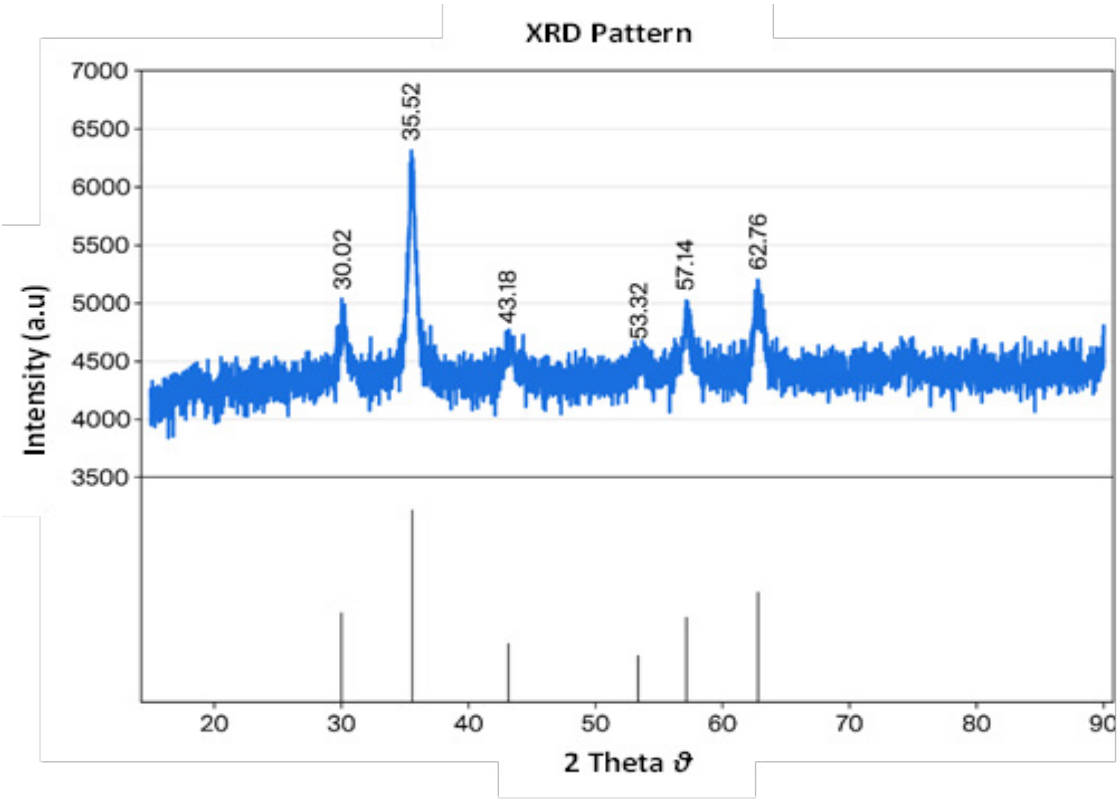

Figure 2: *X-ray diffraction* **(***XRD) pattern for the synthesized MagNPs.*

The XRD analysis was conducted to confirm the crystalline structure of the synthesized MagNPs. The XRD pattern shown in Figure 2 exhibited six diffraction peaks at 2θ of 30.02°, 35.52°, 43.18°, 53.32°, 57.14°, and 62.76°, attributed to Bragg's Planes of 220, 311, 400, 422, 511, and 440, respectively, with an Fd-3m space group of inverse cubic spinel structures of Fe3O4. A close inspection of the diffraction peaks revealed that they were slightly broad, indicating an amorphous nature lacking a periodic structure, which resulted in a broad diffraction pattern with a limited transparency in the X-ray beam. Here, it should be noted that the contribution of the instrumental effects and crystallite shape was essential for size estimation. The diffraction peak widths were extracted from the instrument's profile fitting software, where the broadening due to the instrument was subtracted from the observed peak widths. The calculated NP sizes were found to be in the range of 13-21 nm.

Fourier transform infrared (FT-IR) spectroscopy is a key technique used for elucidating the type of interactions between the MagNPs and the antibiotics in these composites. This technique revealed whether the antibiotic had interacted with the MagNPs surface through physical adsorption or chemical attachment processes. In the first case, the electrostatic /physical adsorption process can be tracked through monitoring the position and shape of the characteristic Fe-O stretching band in the 500-600 cm^{-1} and the stretching and bending of the surface hydroxyl groups at 3400 cm^{-1}, and~1600 cm^{-1} regions, respectively. To confirm the formation of new intermolecular interactions between the individual antibiotics and the synthesized MagNPs in the composite mixtures, FT-IR spectroscopy was employed. Composites were incubated for 21 h, this process was expected to result in their immobilization onto the surface of the MagNPs through polar interactions. To evaluate these intermolecular interactions, FT-IR spectroscopy was used to monitor changes in the position and shape of the Fe-O stretching frequency (υ_{Fe-O}) and the fingerprint region of the individual antibiotics. The FT-IR spectra of the pure MagNPs, individual antibiotics, and their corresponding composites are summarized in Table 1 and displayed in Figure 3a-d.

A characteristic sharp peak corresponding to υ_{Fe-O} in the MagNPs spectrum was observed at 540 cm^{-1}, accompanied by a less intense side peak at 624 cm^{-1}, which is typical for the surface structure of the MagNPs. Additionally, a broad, low-intensity peak at 3464-3192 cm^{-1} was attributed to stretching vibrations of the hydroxyl groups (υ_{O-H}) associated with the weak bending mode (δ_{O-H}) observed at 1681-1610 cm^{-1} (Table 1).

Table 1: *Fourier transform infrared spectroscopy (FT-IR) spectral data for the MagNPs and their composites with Ampicillin, Chloramphenicol, Ciprofloxacin, and Cefoxitin antibiotics.*

Composite	υ_{O-H} (cm^{-1})[a]	υ_{N-H} (cm^{-1})[a]	υ_{C-H} (cm^{-1})	$\upsilon_{C=O}$ (cm^{-1})[b]	$\Delta\upsilon_{C=O}$ (cm^{-1})[c]	$\upsilon_{fun\ gp}$ (cm^{-1})[d]	υ_{Fe-O} (cm^{-1})	$\Delta\upsilon_{Fe-O}$ (cm^{-1})[e]
MagNPs	3464–3192	----	----	----	----	----	624–540	----
Amp.	3244	3038	2904	1785-1615	----	----	----	----
Amp-MagNP	3300	2900	2250–1950	1643	–71	----	570–552	12
Cip	3400	3035	2852	1621	----	1286, C-F	----	----
Cip-MagNP	3500	2950	2400–1950	1643	+22	----	610–590	50
Chl	3214	3071	2928	1714	----	642, C-Cl, 1490, N=O	----	----
Chl-MagNP	3400	2950	2300–1900	1643	–71	----	695–555	15
Cef	3393	3071	2893	1809	----	686, C-S	----	----
Cef-MagNP	3400	2950	2250–1950	1643	–166	----	650–550	10

Where: MagNPs: Magnetite nanoparticles, Amp-MagNP: Ampicillin-MagNP, Cip-MagNP: Ciprofloxacin-MagNP, Chl-MagNP: Chloramphenicol-MagNP, and Cef-MagNP: Cefoxitin-MagNP. υ: stretching vibration frequency, cm^{-1} wavenumber unit, [a]: Overlapping broad band due to υ_{O-H} and υ_{N-H} stretching mode. [b]: Sharp multiple peaks within the fingerprint region due to υC=O / $\upsilon_{C=C}$ stretching and bending modes of O-H/N-H. [c]: ΔυC=O (Shift) = ($\upsilon_{C=O}$ of composite—$\upsilon_{C=O}$ of antibiotic). [d] υfun gp: Frequencies associated with the characteristic functional groups. [e] ΔυFe-O: (Shift) = (υ_{Fe-O} of the composite—υ_{Fe-O} of the MagNP).

The FT-IR images of the individual antibiotics exhibited distinctive bands representing the stretching frequencies of O-H, N-H in the high-frequency region, C=C, C=O within the fingerprint region, and other functional groups, depending on the specific antibiotics, as shown in Figure 3a-d. The key FT-IR features of Amp included the stretching frequencies of O-H and N-H in the range of 3244-3038 cm^{-1}. The C=O frequencies due to lactam and amide appeared at 1850 and 1615 cm^{-1}, overlapping with the bending modes of the hydroxyl (δ_{O-H}) and the amino (δ_{N-H}) groups. However, the FT-IR spectra of Cip exhibited unresolved stretching frequencies due to O-H and N-H in the range of 3400-3035 cm^{-1}, the carbonyl (C=O) group due to carboxylic acid and the quinolone ring, which appeared at about 1621 cm^{-1}, whereas the C-F functional group appeared at 1286 cm^{-1} . The FT-IR spectra of Chl stretching frequencies due to O-H and N-H were observed in the range of 3214-3071cm^{-1}. The $\nu_{C=O}$ of the acylamino group appeared at 1700 cm^{-1}, whereas the $\nu_{N=O}$ and ν_{C-Cl} functional groups appeared at 1490 and 642 cm^{-1}, respectively. The FT-IR spectrum of Cef showed stretching frequencies for its functional groups, including N-H and O-H stretching at around 3393-3071 cm-¹ and an intense C=O stretch from the amide group at about 1750 cm^{-1}. The C=S stretching frequency for Cef was located at 686 cm^{-1}, which typically occurred in the 800-600 range. However, these bands were masked in the spectra of the corresponding MagNPs–antibiotic composites, indicating the formation of intermolecular associations.

To monitor the effect of MagNPs on these frequencies, key spectral regions were examined, specifically those corresponding to the stretching modes of $\upsilon_{C=O}$/ $\upsilon_{C=C}$ combined with the bending modes of δ_{O-H}/ δ_{N-H} and υ_{Fe-O}. It is clear from Figure 3a-d that the characteristic bands of these functional groups were merged in the spectra of the corresponding composites, resulting in broad bands in the regions of 3500-2900, 2400-1900, 1750-1625, and 695-550 cm^{-1}. The large broad band in the 3500-2900 cm^{-1} region was attributed to the existence of H-bonding between the υ_{O-H} and the υ_{N-H} in the structure, as well as the presence of substantial amounts of adsorbed water in the composites. Additionally, sharp bands observed in the 1750–1625 cm^{-1} region and the disappearance of individual antibiotic peaks suggested polar intermolecular interactions within the composites. In the Amp–MagNPs composite, broad and unresolved peaks appeared between 3358-3250 cm^{-1} and 604-507 cm^{-1}, suggesting a strong intermolecular interaction between the ampicillin and the NPs surface. Furthermore, the υ_{Fe-O} band was shifted from 650-570 cm^{-1} in the pure MagNPs to 604-507 cm^{-1} in the Amp-MagNPs composite, confirming the existence of strong physicochemical interactions, likely including remarkable H-bonding. Similar shifts were observed in the FT-IR spectra of the Chl-MagNPs, Cip-MagNPs, and Cef-MagNPs, although the extent of the shifts varied.

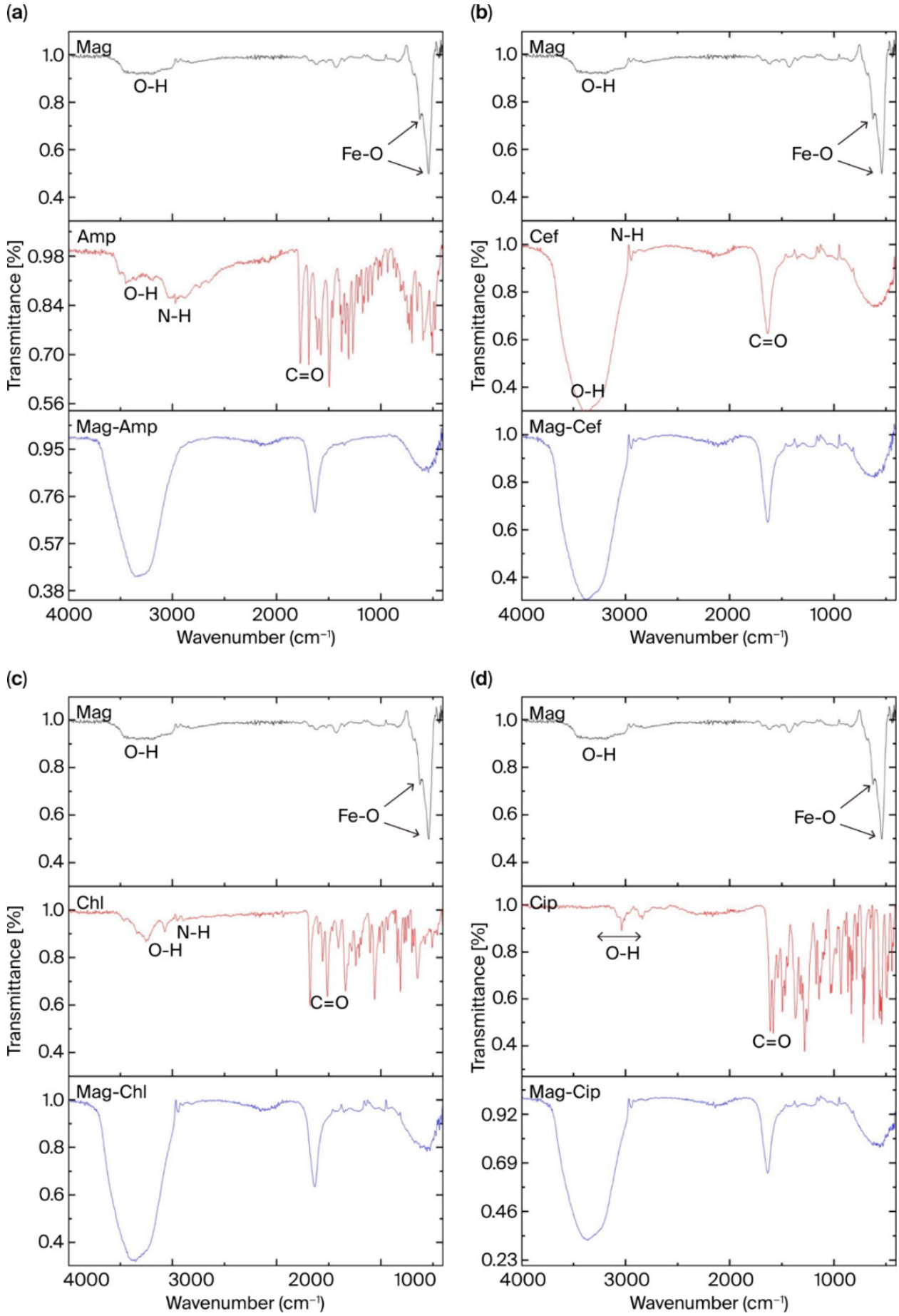

Figure 3: *Fourier transform infrared spectroscopy* **(***FT-IR) spectra of the prepared magnetite nanoparticles (MagNPs); (a) Ampicillin (Amp) and the MagNPs-Amp composite; (b) Cefoxitin (Cef) and the MagNPs-Cef composite; (c) Chloramphenicol (Chl) and the MagNPs-Chl composite; (d) Ciprofloxacin (Cip) and the MagNPs-Cip composite.*

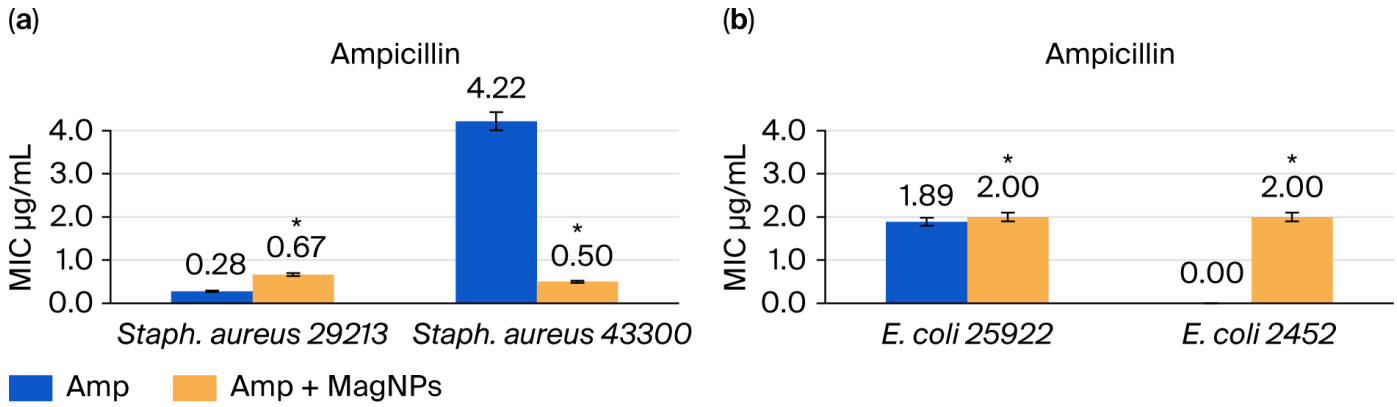

Figure 4: *Minimal inhibitory concentration (MIC) values for Ampicillin (Amp) without and with MagNPs against (a) Staph. aureus and (b) E. coli. The results are represented as mean values of n= 9 replicate, the error bars indicate the standard error of these replicates. (*) indicates p-value ≤ 0.01 using the nonparametric Kruskal–Wallis and Wilcoxon rank test.*

The υ_{Fe-O} bands for these composites appeared in the ranges of 677-585cm^{-1}, 660-562cm^{-1}, and 702-521 cm^{-1}, respectively. Additionally, broad υ_{O-H} stretching bands were observed at 3500-3200 cm^{-1} in all the composites indicating the presence of H-bonding and substantial amounts of adsorbed water. The sharp bands at 1633 cm^{-1} recorded in all the spectra corresponded to the bending mode of OH groups, which was often combined with the stretching vibrations of C=C ($\upsilon_{C=C}$) and/or C=O ($\upsilon_{C=O}$) from the antibiotics.

The $\Delta\upsilon_{C=O}$ showed that upon the composite formation of the Amp, Chl, and Cef antibiotics with the MagNPs, a considerable $\nu_{C=O}$ shift of about 166 - 71 cm^{-1} was observed in the lower frequency IR region, as summarized in Table 1. On the contrary, the observed change in the Cip-MgNPs compared to that of the Cip occurred at a higher frequency of about 22 cm^{-1}. Furthermore, the observed change in the Fe-O stretching frequency ($\Delta\upsilon_{Fe-O}$) was indicative of the interaction strength, as shown in Table 1. The observed moderate shifts in Amp-MagNPs ($\Delta\upsilon_{Fe-O}$ = 12 cm^{-1}), Cef-MagNPs ($\Delta\upsilon_{Fe-O}$ =10 cm^{-1}), and Chl-MagNPs ($\Delta\upsilon_{Fe-O}$ = 15 cm^{-1}) inferred weak interaction forces, unlike the change in Cip-MagNPs ($\Delta\upsilon_{Fe-O}$ = 50 cm^{-1}), which indicated strong interactions. These shifts suggested the existence of polar intermolecular forces among the polar sites of the given antibiotic molecules and the MagNPs.

This conclusion was further supported by the merging of vibrational modes associated with H-bonding interactions, as indicated by the positions of the O–H and the N–H stretching bands (υ_{O-H} / υ_{N-H}). However, in chemical conjugation, new IR bands emerged, suggesting a strong interaction involving specific groups. This effect can be monitored by a close inspection of the broad features observed in the composites but not in the components in the 2000-2400 cm^{-1} region. The emerged broad bands as depicted in Figure 3a-d and summarized in Table 1 showed that the interaction was purely a simple physical process and was combined with the coexistence of specific interactions within the C=C/C=O conjugation system.

Determination of minimal inhibitory concentration (MIC) and minimal bactericidal concentration (MBC)

The antibacterial efficacy of the MagNPs–antibiotic composites against four bacterial strains (*Staph. aureus* and *E. coli*) was assessed by determining their MICs and MBCs. The 21-hour incubation period was selected to maximize the interaction between the antibiotics and MagNPs. Compared to a 1-hour mixing period, 21 h period showed a greater antibacterial activity. The obtained results are illustrated in Figures 4-7 and Table 2. The results showed a substantial antibacterial effect of the Amp-MagNPs composite against all the tested strains (p-value = 0.0087), as illustrated in Figure 4. Notably, the MIC value for the MRSA strain *Staph. aureus* (ATCC 43300) was dramatically reduced from 4.22 µg/ml to 0.5 µg/ml, indicating remarkably enhanced antibacterial activity of the composite against this resistant strain. Although the MDR strain of *E. coli* (BAA 2452) was resistant to ampicillin alone, its MagNPs-Amp composite enhanced its antibacterial potential. This composite considerably lowered the MIC values across all the tested strains (p-value = 0.0095).

Similarly, the MagNPs-Cef composite displayed an improved antibacterial activity (Figure 5). The MIC values were reduced by four-fold, eight-fold, and two-fold for *Staph. aureus* ATCC 29213, MRSA *Staph. aureus* ATCC 43300, and *E. coli* ATCC 25922, respectively, indicating that lower antibiotic concentrations were required to inhibit the bacterial growth when combined with the MagNPs. The contribution of the MagNP to this enhancement was statistically significant (p-value of 0.02), suggesting that the incorporation of MagNPs increased the antibacterial efficacy of the cefoxitin.

The MagNPs-Chl composite demonstrated a strong antibacterial activity against all the tested strains, significantly lowering the MIC values (p-value < 0.0001). MIC values for both *Staph. aureus* strains were reduced eight-fold, and the wild-type *E. coli* strain expressed a two-fold decrease. However, the MDR *E. coli* strain remained resistant to the MagNPs-Chl composite (Figure 6). Despite this, the addition of MagNP still significantly enhanced the antibacterial potential of the chloramphenicol (p-value = of 0.039).

Table 2: *Minimal bactericidal concentration values of MagNPs alone (mg/ml), antibiotics (µg/ml), and MagNPs–antibiotic composites against wild-type and multi-drug resistant (MDR) strains of Staphylococcus aureus and Escherichia coli.*

#	Conc. (µg/ml)/ Agents	*Staph. aureus* 29213	*Staph. aureus* 43300	*E. coli* 25922	*E. coli* 2452
		MBC	MBC	MBC	MBC
1	MagNP	ND	ND	NP	NP
2	Amp	0.25	4.00	4.00	NP
3	Amp + MagNP	ND	2.00	ND	ND
4	Cef	4.00	32.00	4.00	64.00
5	Cef + MagNP	ND	8.00	ND	ND
6	Chl	4.00	4.00	4.00	4.00
7	Chl + MagNP	4.00	2.00	4.00	4.00
8	Cip	2.00	32.00	1.00	1.00
9	Cip + MagNP	ND	4.00	ND	ND

Where: MagNPs: Magnetite nanoparticles, Amp-MagNP: Ampicillin-MagNP, Cef-MagNP: Cefoxitin-MagNP, Chl-MagNP: Chloramphenicol-MagNP and Cip-MagNP: Ciprofloxacin-MagNP; MBC: Minimal bactericidal concentration values; ND: not determined; NP: not performed due to no minimal inhibitory concentration value detected.

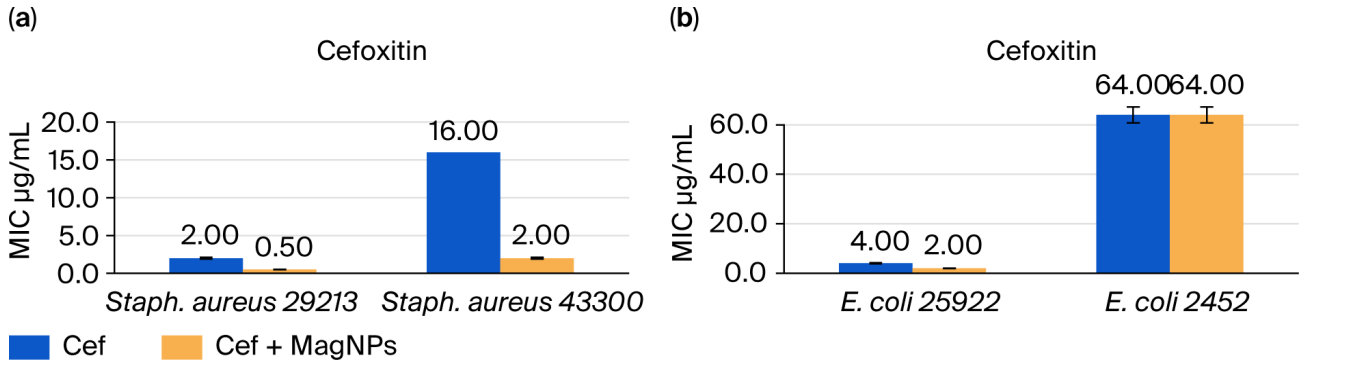

Figure 5: *Minimal inhibitory concentration (MIC) values for Cefoxitin (Cef) without and with MagNPs against (a) Staph. aureus and (b) E. coli. The results are represented as mean values of n= 9 replicate, the error bars indicate the standard error of these replicates.*

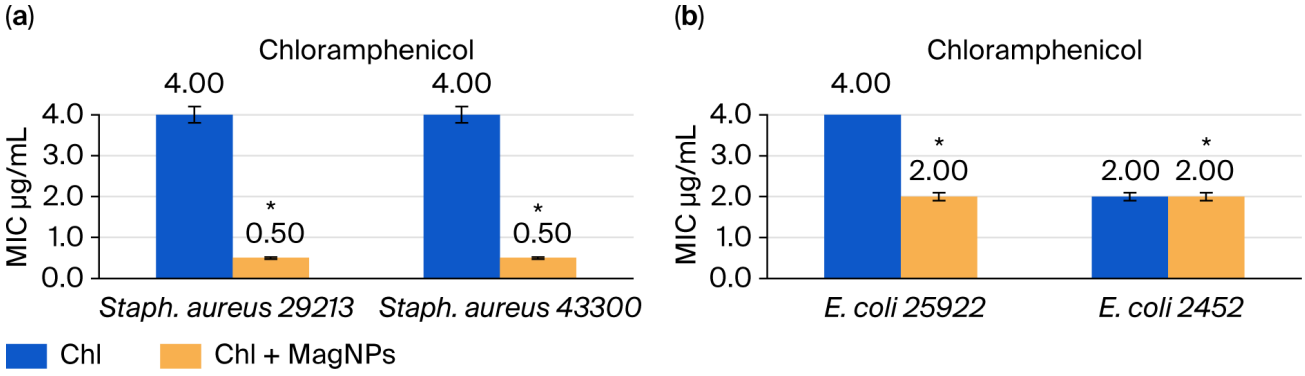

Figure 6: *Minimal inhibitory concentration (MIC) values for Chloramphenicol (Chl) without and with MagNPs against (a) Staph. aureus and (b) E. coli. The results are represented as mean values of n= 9 replicate, the error bars indicate the standard error of these replicates. (*) indicates p-value ≤ 0.01 using the nonparametric Kruskal–Wallis*

test and Wilcoxon rank test.

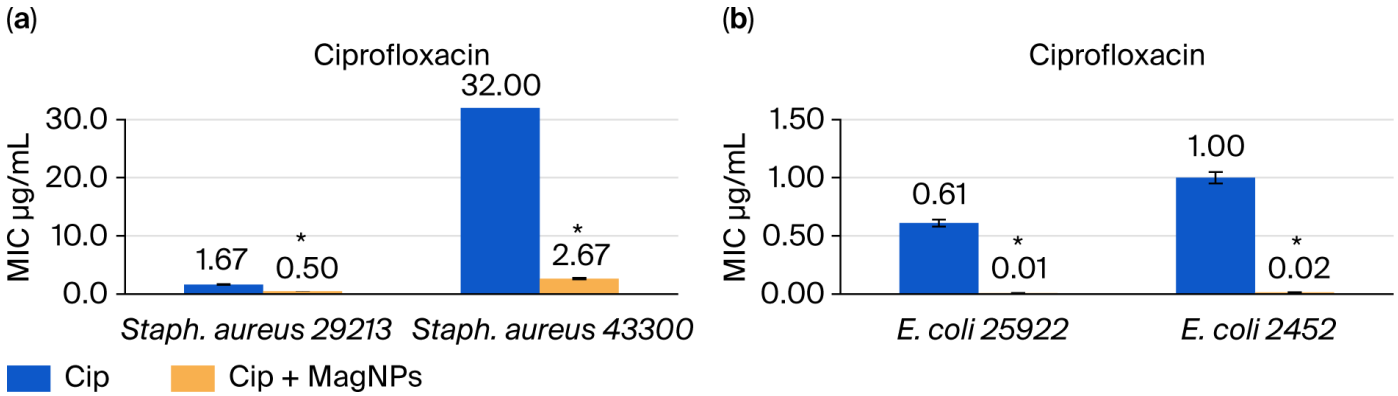

Figure 7: *Minimal inhibitory concentration (MIC) values for Ciprofloxacin (Cip) without and with MagNPs against (a) Staph. aureus and (b) E. coli. The results are represented as mean values of n= 9 replicate, the error bars indicate the standard error of these replicates. (*) indicates p-value ≤ 0.01 using the nonparametric Kruskal–Wallis test and Wilcoxon rank test.*

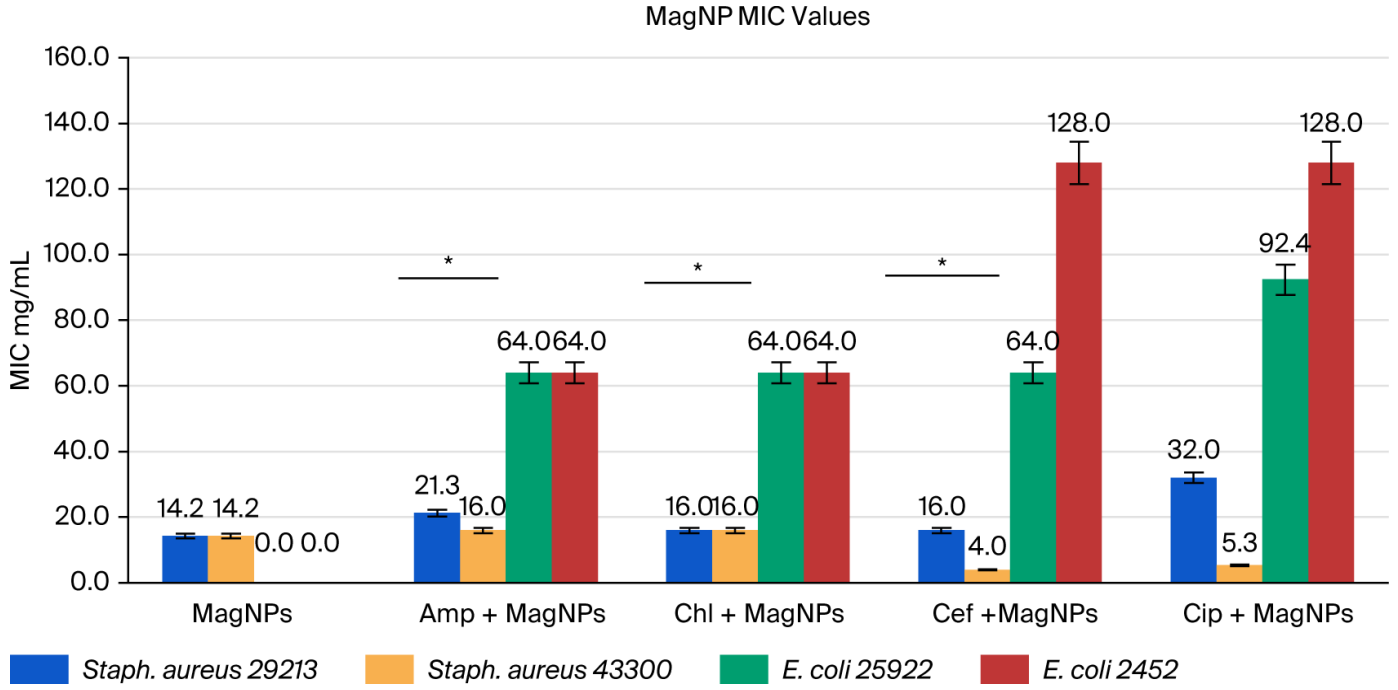

Figure 8: *Minimal inhibitory concentration (MIC) values for the MagNPs and MagNPs combined with the different antibiotics against Staph. aureus and E. coli strains. The results are represented as mean values of n= 9 replicate, the error bars indicate the standard error of these replicates. (*) indicates p-values for the MagNPs MIC values (with Amp < 0.01, with Chl < 0.05, and with Cef < 0.05) using the Wilcoxon rank test.*

The MagNPs-Cip composite also exhibited a significant antibacterial activity against all the tested strains (p-value of 0.0022). The MIC for the ciprofloxacin-sensitive *Staph. aureus* strain decreased from 1.67µg/ml to 0.5µg/ml, while the MIC for the MRSA strain decreased from 32µg/ml to 2.67µg/ml, suggesting a substantial improvement in ciprofloxacin activity against the tested strains. The MagNPs-Cip composite displayed remarkable antibacterial effects, achieving up to a 60-fold reduction in the MICs against both *E. coli* strains, compared to the Cip antibiotic alone (Figure 7).

To evaluate their antibacterial efficacy, MIC values for the MagNPs alone and when combined with the different antibiotics are shown in Figure 8. The illustration exhibited a significant reduction in MIC values for MagNPs against both *Staph. aureus* strains when they were combined with Amp, Cef, and Chl, with p-values < 0.009 for Amp, < 0.0200 for Cef, and < 0.0392 for Chl. Furthermore, the MRSA strain was affected by the MagNPs-Cip composite. In contrast, *E. coli* strains that were not affected by the MagNPs

alone were affected by the composites with all the antibiotics used.

The MBCs were also evaluated against both the wild-type and the antibiotic-resistant strains. As shown in Table 2, all the tested antibiotics exhibited bactericidal activity, except against the MDR *E. coli* strain. Notably, the MagNPs-Chl composite retained a bactericidal potential across all the tested strains, even at lower concentrations. In contrast, the other antibiotic composites exhibited primarily bacteriostatic effects. Interestingly, the MRSA strain displayed reduced MBC values when treated with the antibiotics combined with the MagNPs, unlike the other strains. In the cases where the MICs were not obtained for certain composites, the MBC was recorded (Table 2). These results suggested that while MagNPs–antibiotic composites exhibited an inhibitory activity; however, in some cases, the reduced concentrations may be insufficient to achieve the bactericidal effects, allowing for bacterial survival.

In summary, the results of this study highlighted the potential of combining antibiotics with MagNPs to considerably reduce the MIC values for the wild-type *Staph. aureus* and *E. coli* strains, while also enhancing their antibacterial efficacy against the resistant strains such as MRSA and MDR *E. coli*. These findings support the use of MagNPs in the form of a combination therapy as a promising approach to improving their antibacterial efficacy and addressing the growing challenge of antibiotic resistance. However, the present findings are limited to *in vitro* observations, however, further toxicity, biocompatibility, and *in vivo* studies are needed before clinical relevance can be established.

Discussion

Given the global increase in bacterial resistance, there is an urgent need for innovative solutions to address this pressing issue. This study explored the strategies used to reinstate the bactericidal efficacy of the older-generation antibiotics, including ampicillin, cefoxitin, chloramphenicol, and ciprofloxacin, which had diminished due to the development of resistance, by combining them with MagNP and evaluating their potential to enhance the antibacterial activity. We envisaged that this approach would combat resistance and restore therapeutic effectiveness against both wild-type and MDR *Staph. aureus* and *E. coli* ATCC strains. This work is consistent with the contemporary initiatives used to re-establish the therapeutic value of the established antibiotics through MagNP–antibiotic composite formulation strategies (Mazraeh *et al*., 2022; Sharma *et al*., 2025). It may serve as a practical intervention in resource-constrained healthcare environments with restricted availability of advanced antimicrobials. By improving the performance of the current antimicrobial agents instead of focusing only on creating new ones, the current methodology delivered a cost-efficient and broadly applicable means of addressing the escalating issue of antimicrobial resistance. In addition, these tactics may speed up the clinical use, since these agents possess thoroughly documented safety and pharmacological profiles as previously documented (Venter, 2019; Parvin *et al*., 2025).

In the present work, MagNPs were synthesized using a coprecipitation method with continuous sonication, and the MagNP were characterized using SEM, XRD, and FT-IR physical assays. The SEM images revealed that the spherical NPs were well-formed and of uniform size and shape (spherical). Using Scherrer's equation, the XRD analysis validated that the obtained NPs were composed of well-defined 20 nm crystallites, with a peak structure consistent with the XRD standard data card (JCPDS NO. 01-071-6336) in the previous studies (Zhang *et al*., 2019; Petcharoen and Sirivat, 2012; Alomari *et al*., 2015; Saqib *et al*., 2018), confirming the effectiveness of the coprecipitation method at producing well-defined MagNPs, despite variations in the specific methodologies employed.

Fourier transform infrared (FT–IR) spectroscopy analysis confirmed the structural integrity of the synthesized MagNPs, by identifying a sharp, characteristic stretching band at 540 cm^{-1}, along with a less intense side peak at 624 cm^{-1}. These peaks were typically consistent with the surface structure of MagNPs, as previously reported by different authors for the 650-570 cm^{-1} range (Current *et al*., 2017; Chavan *et al*., 2020). The FT-IR analysis revealed strong interactions between the NPs and antibiotics, mainly through hydrogen bonding. The observed shifts in the FT-IR bands suggested the existence of interactions between the antibiotics and the MagNP surface, likely involving hydrogen bonding and other polar intermolecular interactions. These interactions are crucial since the resulting NP–antibiotic composites are suggested to enhance

stability, solubility, and bioavailability in the living microorganisms (Sterren *et al*., 2017; Chavan *et al*., 2020). Given that the NP's size, charge, and morphology strongly influence biological behavior and antimicrobial activity, the uniform particle size and crystalline stability observed here likely contributed to an enhanced antibiotic performance (Venter, 2019; Sharaf *et al*., 2022). However, FT-IR analysis alone does not allow definitive identification of the binding mechanism or distinction between simple adsorption and stronger surface interactions. A limitation of the present study is that the exact nature of the interaction between the antibiotics and the MagNPs was not determined. Although the FT-IR data support the existence of physicochemical interactions, further characterization techniques, such as ZP measurements, thermogravimetric analysis, or surface spectroscopy, would be required to better elucidate the binding mechanism and distinguish between adsorption and stronger surface interactions.

This study had also revealed that MagNPs alone inhibited the growth of both strains of *Staph. aureus*, with MIC value of 14 mg/ml, which is consistent with several previous studies (Tran *et al*., 2010; Bataineh *et al*., 2024). However, no effects were observed in relation to the growth of both wild-type and MDR strains of *E. coli*. The absence of activity against *E. coli* was plausibly attributed to the robust outer membrane of the Gram-negative bacteria, which serves as a selective barrier, restricting NPs penetration and thereby reducing the intracellular targeting (Nikaido, 2003). This finding contrasts with previous studies that highlighted the inhibitory activity of MagNPs against different *E. coli* strains (Auffan *et al*., 2008; Al-Shabib *et al*., 2018). It is well known that MagNPs mechanism of action for inhibiting the bacterial growth involves disrupting the integrity of the cell wall, hindering DNA and enzyme synthesis, and generating reactive oxygen species (ROS) within the cell (Hosseinzadeh, 2025). While these mechanisms may explain the enhanced antibacterial activity observed, they were not directly evaluated in the present study and therefore remain speculative. Further studies are needed to clarify the specific mechanisms of action through which these MagNPs exert their effects on the various bacterial strains.

When MagNPs were combined with antibiotics, remarkable reductions in the MIC values for Amp, Cef, Chl, and Cip were observed, indicating that effective bacterial growth inhibition could be achieved at lower antibiotic concentrations. Although marked reductions in MIC values were observed following combination with MagNPs, formal synergy testing was not performed. Therefore, the results should be interpreted as enhanced antibacterial activity rather than definitive evidence of synergy. This suggests that combining the MagNPs with the antibiotics is a promising strategy for enhancing the efficacy of the older-generation antibiotics, especially against the MDR strains. To the best of our knowledge, this is the first study to evaluate the antibacterial activity of the present MagNPs–antibiotic composites against MDR *E. coli* BAA 2425 and methicillin resistant *Staph. aureus* (MRSA) ATCC 43300. Among the tested composites, the MagNPs-Amp demonstrated the most substantial effects, with statistically notable reductions in MIC values across all the bacterial strains assessed in this study. This indicated that MagNPs may help restore the antibacterial activity of the antibiotics that have become less effective due to resistance. Indeed, a marked enhancement in antibacterial activity was observed for the exposure of MRSA *Staph. aureus* ATCC 43300 to this composite, with an eight-fold decrease in the MIC, which dramatically enhanced the potency of ampicillin against this MDR strain. These findings suggest that MagNPs improve intracellular drug delivery, suppress efflux mechanisms, and possibly overcome phenotypic resistance. The associated drop in MIC values suggested that this combinations led to lower effective antibiotic doses, which may help minimize the adverse effects and slow the development of antibiotic resistance (Venter, 2019).

The observations herein confirmed that Amp was completely ineffective against MDR *E. coli* BAA 2452, which is consistent with the established profile of this strain, known to be resistant to both carbapenem and β-lactam antibiotics (Nordmann *et al*., 2009). However, the successful restoration of Amp susceptibility by the MagNPs-Amp composite indicated the crucial function of the NPs due to their physicochemical properties, including their possible influence as antibacterial agents, avoidance of the active efflux system, and overwhelming of the resistance machinery (Venter, 2019; Sharaf *et al*., 2022). These findings suggest that MagNPs may influence the characteristics of the microbial cell walls or the membrane structures, potentially enhancing

their permeability to antibiotics (Gholami *et al.*, 2018; Abo-Zeid and Williams, 2020; Armijo *et al.*, 2020). Moreover, the antibiotics' modes of action on the bacterial cells involved interfering with cell wall synthesis, inhibiting protein building, and disrupting DNA replication (Ahmed *et al.*, 2023). These mechanisms were expected to act in concert with the antibacterial activity of MagNPs, resulting in enhanced inhibition of bacterial growth. These findings support the enhanced antibacterial efficacy of the composite through multiple mechanisms, in addition to the role of MagNPs in boosting the existing antibiotics to overcome the antibiotic resistance crisis.

Composites of cefoxitin and MagNPs likewise showed considerably greater antibacterial properties, reducing the MIC values for *Staph. aureus* ATCC 29213, MRSA *Staph. aureus* ATCC 43300, and *E. coli* ATCC 25922 by two-fold, three-fold, and one-fold, respectively. Thus, MagNPs also augmented the antibacterial efficacy of the cefoxitin, lowering the therapeutic dose without compromising its effectiveness.

A significant reduction in the MIC was also observed with the MagNPs-Chl composite for both the wild-type and MDR *Staph. aureus* strains, as well as the wild-type *E. coli* strain (p-value < 0.0001). Specifically, the MIC values for both *Staph. aureus* strains were reduced by eight-fold, while the wild-type *E. coli* strain exhibited a two-fold decrease. However, the MDR *E. coli* strain remained relatively resistant to the MagNPs-Chl composite, requiring further investigation to elucidate whether this was due to the additional outer membrane barrier in the *E. coli* envelope or possibly due to more robust systems that actively pump the antimicrobials out of *E. coli* compared to *Staph. aureus*. This observation likely reflected the potent efflux machinery in MDR *E. coli* (e.g., AcrAB–TolC) that expelled the antibiotic–MgaNPs complexes, suggesting the need for further studies to explore the combination of NP's therapy with the efflux pump inhibitors (Alenazy, 2022). To the best of our knowledge, this is the first work to investigate the effects of mixing MagNPs–antibiotic composites for 21 h, highlighting the novelty and uniqueness of the present study. These results were supported by the FT-IR analysis, which showed the intermolecular interactions between the MagNPs and the antibiotics in the prepared composites.

The observed disparity in the antibacterial efficacy between the 21-h mixing protocol and both the 1-h mixing and the checkerboard assay trials (results not shown) confirmed the critical role of the incubation duration for enhancing the antibacterial activity of the MagNPs–antibiotic composites (Current *et al.*, 2017; Gholami *et al.*, 2018). The greater antibacterial activity observed after 21 h of mixing compared with 1 h suggests that prolonged contact between the antibiotics and the MagNPs may promote more effective interactions between the two components. The extended 21-h mixing period likely facilitated a more effective immobilization of antibiotics on the surface of MagNPs through non-covalent interactions. These findings stressed that the method of preparing the nano-antibiotic combinations was critical, suggesting that pre-formed nano-therapeutic complexes could be developed as stable, ready-to-use clinical formulations rather than requiring fresh preparation before each use. This extended interaction promoted a stronger surface adhesion and an increased stability, leading to a reduction in the MIC values against the tested bacterial strains. On the contrary, short-term mixing (1 h) and checkerboard methods appeared insufficient for achieving such antibiotic immobilization, resulting in markedly lower or absence of enhancements in antibacterial activity. The FT–IR analysis further supported this conclusion, revealing that the antibiotics interact with the surface of the MagNPs primarily through H-bonding *via* hydroxyl groups. This binding mechanism agrees with several previous reports (Current *et al.*, 2017; Gholami *et al.*, 2018; Chavan *et al.*, 2020), which involved FeNPs and stabilizing agents Figure 3a-d. Collectively, these results confirmed that prolonged incubation enabled sufficient antibiotic immobilization onto MagNP's surface, which was crucial for optimizing the antibacterial efficacy of the composites (Current *et al.*, 2017). These findings are promising for future applications aiming at combating the MDR bacterial strains. However, further studies are required to understand the exact mechanisms underlying this enhanced antibacterial activity.

The current findings agree with recent studies, which supported the idea that metal oxide NPs (MONPs) can increase the antimicrobial efficacy of the antibiotics (Tyers and Wright, 2019; Wang *et al.*, 2022). The general antimicrobial activity of the MONPs is reported to arise from multiple mechanisms, including oxidative damage, disruption

of microbial cell membranes, interference with metal ion homeostasis, protein and enzyme dysfunction, genotoxicity, and photo-killing, with the specific mechanisms varying based on the nature and the chemistry of the MONPs (Raghunath and Perumal, 2017; Hosseinzadeh, 2025).

The present study's perspective emphasized the importance of the combination therapy, a strategy initially proposed by (Mouton, 1999), where the use of two or more antibiotics together can help prevent the bacteria from developing resistance. By targeting the bacteria with multiple agents simultaneously, the combination therapy makes it more difficult for them to evade treatment (Mouton, 1999). In this study, combining MagNPs with antibiotics had increased the efficacy of the older-generation antibiotics against the MDR bacteria. A bonus effect is that a combination therapy may help prevent the development of resistance to these composites (Mouton, 1999). Moreover, this innovative approach not only increased the therapeutic potential of the existing antibiotics but also paved the way for more effective treatment strategies in the fight against the antibiotic-resistant pathogens.

Overall, these findings support the MagNPs-augmented antibiotic composites as a viable complementary approach to restore the activity of the existing antimicrobials, preserve their clinical value, and reinforce the global strategies to combat the antimicrobial resistance.

Conclusions

Antibiotic resistance is emerging as a serious challenge for researchers, intensifying the need to find alternative solutions. Natural materials, either nanoparticles or plant extracts, could produce some inhibitory effects on bacterial growth. However, when antibiotics are combined with these materials, their antibacterial activity can be enhanced, representing a novel strategy for addressing the pressing issue of antibiotic resistance. This revival of interest is driven by the escalating need to develop new treatment approaches that are effective against multi drug-resistant pathogens, especially in clinical environments where traditional antimicrobial agents are losing effectiveness. Nanoparticles, characterized by their unique structural, chemical, and antimicrobial properties, are increasingly recognized as valuable complementary agents, capable of enhancing antibiotic bioavailability, cellular uptake, and overall antimicrobial effectiveness. Exploring these composites against different bacterial strains could enhance antimicrobial therapy and provide a more efficient approach. MagNPs–antibiotic composites in addition to older-generation antibiotics have the potential to improve antibiotics' efficacy against multi-drug-resistant strains. Further research is needed to elucidate the *in vitro* and *in vivo* molecular mechanisms underlying the enhanced antibacterial activity of the MagNPs–antibiotic composites to optimize their design and achieve better performance. This strategy seeks to strengthen antibiotic potency at reduced doses, shorten treatment durations, and diminish the likelihood of further antimicrobial resistance development. While calls for innovative solutions to combat bacterial resistance are growing, a practical approach may lie in combining antibiotics with nanoparticles, particularly older-generation antibiotics that remained effective for many years before widespread bacterial resistance has emerged.

Acknowledgement

The authors acknowledge the Deanship of Research in Jordan University of Science and Technology for the financial support.

Novelty Statement

Magnetite nanoparticles (MagNP)-antibiotic composites represent a novel strategy for overcoming multidrug resistance. By leveraging interactive effects, these MagNP-based systems enhance the efficacy of older–generation antibiotics against the resistant bacterial strains, while offering a potent alternative to the development of entirely new drug classes.

Author's Contribution

Sereen M.B. Bataineh: Conceptualization, methodology, validation, investigation, resources, writing—review and editing, visualization, supervision, project administration, and funding acquisition.
Samya M. Abu-Zreg: Methodology, formal analysis, investigation, data curation, writing—original draft, writing—review and editing, and visualization.
Isam M. Arafa: Conceptualization, methodology, validation, investigation, resources, writing—original draft, writing—review and editing, visualization, and

supervision.

Hanan M. Hammouri: Software, data curation, and writing—review and editing.

Homa Darmani: Writing—original draft, and writing—review and editing.

All authors have read and agreed to the published version of this manuscript.

Funding source

This work was funded by the Deanship of Research at Jordan University of Science and Technology (Grant Number 556/2020).

Generative AI and AI assisted technology statement

The authors declare that no generative AI and AI assisted technology was used in the creation of this manuscript.

Conflict of interests

The authors have declared no conflicts of interest.

References

Abo-zeid, Y. and Williams, G.R., 2020. The potential anti-infective applications of metal oxide nanoparticles: A systematic review. Wiley Interdiscip. Rev. Nanomed. Nanobiotechnol., 12: 1–36. https://doi.org/10.1002/wnan.1592

Abu-Dalo, M., Jaradat, A., Albiss, B.A. and Al-Rawashdeh, N.A.F., 2019. Green synthesis of TiO2 NPs/pristine pomegranate peel extract nanocomposite and its antimicrobial activity for water disinfection. J. Environ. Chem. Eng., 7: 103370. https://doi.org/10.1016/j.jece.2019.103370

Ahire, J.J. and Dicks, L.M.T., 2016. Antimicrobial hyaluronic acid–cefoxitin sodium thin films produced by electrospraying. Curr. Microbiol., 73: 236–241. https://doi.org/10.1007/s00284-016-1057-1

Ahmed, S., Ahmed, M.Z., Rafique, S., Almasoudi, S.E., Shah, M., Jalil, N.A.C. and Ojha, S.C., 2023. Recent approaches for downplaying antibiotic resistance: Molecular mechanisms. Biomed. Res. Int., 2023. https://doi.org/10.1155/2023/5250040

Alenazy, R., 2022. Drug efflux pump inhibitors: A promising approach to counter multidrug resistance in gram-negative pathogens by targeting AcrB protein from AcrAB-TolC multidrug efflux pump from *Escherichia coli*. Biology (Basel). 11. https://doi.org/10.3390/biology11091328

Alomari, A., Ghanem, H.M.E., Lehlooh, A., Arafa, I.M., Bsoul, I. and Batra, A., 2015. Mössbauer, VSM and X-ray diffraction study of Fe3O4 (NP's)/PVOH for biosensors applications. Sensors Transd., 192: 53–60.

Al-Shabib, N.A., Husain, F.M., Ahmed, F., Khan, R.A., Khan, Mohammad Shavez, Ansari, F.A., Alam, M.Z., Ahmed, M.A., Khan, Mohd Shahnawaz, Baig, M.H., Khan, J.M., Shahzad, S.A., Arshad, M., Alyousef, A. and Ahmad, I., 2018. Low temperature synthesis of superparamagnetic iron oxide (Fe3O4) nanoparticles and their ROS mediated inhibition of biofilm formed by food-associated bacteria. Front. Microbiol., 9: 2567. https://doi.org/10.3389/fmicb.2018.02567

Armijo, L.M., Wawrzyniec, S.J., Kopciuch, M., Brandt, Y.I., Rivera, A.C., Withers, N.J., Cook, N.C., Huber, D.L., Monson, T.C., Smyth, H.D.C. and Osiński, M., 2020. Antibacterial activity of iron oxide, iron nitride, and tobramycin conjugated nanoparticles against Pseudomonas aeruginosa biofilms. J. Nanobiotechnol., 18: 1–27. https://doi.org/10.1186/s12951-020-0588-6

Auffan, M., Achouak, W., Rose, J., Roncato, M.A., Chanéac, C., Waite, D.T. and Bottero, J.Y., 2008. Relation between the redox state of iron-based nanoparticles and their cytotoxicity toward *Escherichia coli*. Environ. Sci. Technol., 42: 6730–6735. https://doi.org/10.1021/es800086f

Bataineh, S.M.B., Arafa, I.M., Abu-Zreg, S.M., Al-Gharaibeh, M.M., Hammouri, H.M., Tarazi, Y.H. and Darmani, H., 2024. Synergistic effect of magnetic iron oxide nanoparticles with medicinal plant extracts against resistant bacterial strains. Magnetochemistry, 10. https://doi.org/10.3390/magnetochemistry10070049

Bhattacharya, P. and Neogi, S., 2017. Gentamicin coated iron oxide nanoparticles as novel antibacterial agents. Mater. Res. Express, 4. https://doi.org/10.1088/2053-1591/aa8652

Chavan, C., Kamble, S., Murthy, A.V.R. and Kale, S.N., 2020. Ampicillin-mediated functionalized gold nanoparticles against ampicillin-resistant bacteria: Strategy, preparation and interaction studies. Nanotechnology, 31. https://doi.org/10.1088/1361-6528/ab72b4

Clinical and Laboratory Standards Institute (CLSI), 2020. Performance standards for antimicrobial susceptibility testing. West Valley

Road, Suite 2500, Wayne, Pennsylvania 19087 USA.

Cook, M.A. and Wright, G.D., 2022. The past, present, and future of antibiotics. Sci. Transl. Med., 14: 1–12. https://doi.org/10.1126/scitranslmed.abo7793

Corona, A., De Santis, V., Agarossi, A., Prete, A., Cattaneo, D., Tomasini, G., Bonetti, G., Patroni, A. and Latronico, N., 2023. Antibiotic therapy strategies for treating gram-negative severe infections in the critically Ill: A narrative review. Antibiotics, 12: 1–30. https://doi.org/10.3390/antibiotics12081262

Current, K.M., Dissanayake, N.M. and Obare, S.O., 2017. Effect of iron oxide nanoparticles and amoxicillin on bacterial growth in the presence of dissolved organic carbon. Biomedicines, 5. https://doi.org/10.3390/biomedicines5030055

Dizaj, S.M., Lotfipour, F., Barzegar-Jalali, M., Zarrintan, M.H. and Adibkia, K., 2014. Antimicrobial activity of the metals and metal oxide nanoparticles. Mater. Sci. Eng. C, 44: 278–284. https://doi.org/10.1016/j.msec.2014.08.031

European Committee for Antimicrobial Susceptibility Testing (EUCAST) of the European Society of Clinical Microbiology and Infectious Diseases (ESCMID), 2003. Determination of minimum inhibitory concentrations (MICs) of antibacterial agents by broth dilution. Clin. Microbiol. Infect., 9(8). https://doi.org/10.1046/j.1469-0691.2003.00790.x

Ezealigo, U.S., Ezealigo, B.N., Aisida, S.O. and Ezema, F.I., 2021. Iron oxide nanoparticles in biological systems: Antibacterial and toxicology perspective. JCIS Open, 4: 100027. https://doi.org/10.1016/j.jciso.2021.100027

Gholami, A., Ebrahiminezhad, A., Abootalebi, N. and Ghasemi, Y., 2018. Synergistic evaluation of functionalized magnetic nanoparticles and antibiotics against *Staphylococcus aureus* and *Escherichia coli*. Pharm. Nanotechnol., 6: 276–286. https://doi.org/10.2174/2211738506666181031143048

Grooters, K.E., Ku, J.C., Richter, D.M., Krinock, M.J., Minor, A., Li, P., Kim, A., Sawyer, R. and Li, Y., 2024. Strategies for combating antibiotic resistance in bacterial biofilms. Front. Cell. Infect. Microbiol., 14: 1–7. https://doi.org/10.3389/fcimb.2024.1352273

Han, Q., Wang, L., Li, J., Dong, Y., Ma, Y., Zhang, J. and Yu, S., 2025. Built-in field-driven S-scheme boron-doped nanodiamond/TiO2(101)/MXene photocatalyst for efficient antibiotic elimination: Mechanisms and DFT validation. Chem. Eng. J., 519: 165290. https://doi.org/10.1016/j.cej.2025.165290

Hosseinzadeh, H., 2025. Antibacterial/ magnetic iron oxide nanoparticles: A comprehensive review of synthesis methods, doping effects, antibacterial properties, and applications in medical and food industries. J. Appl. Mater. Sci., 1: 1–32.

Joseph, J., 2023. Titanium dioxide nanoparticles: Prospects and applications in nanotheranostics. Nanomaterials, 10: 253–278. https://doi.org/10.1016/B978-0-323-85784-0.00010-8

Karaagac, O., Kockar, H. and Tanrisever, T., 2011. Properties of iron oxide nanoparticles synthesized at different temperatures. J. Supercond. Nov. Magn., 24: 675–678. https://doi.org/10.1007/s10948-010-0932-4

Khezerlou, A., Alizadeh-Sani, M., Azizi-Lalabadi, M. and Ehsani, A., 2018. Nanoparticles and their antimicrobial properties against pathogens including bacteria, fungi, parasites and viruses. Microb. Pathog., 123: 505–526. https://doi.org/10.1016/j.micpath.2018.08.008

Kim, J.S., Kuk, E., Yu, K.N., Kim, J.H., Park, S.J., Lee, H.J., Kim, S.H., Park, Y.K., Park, Y.H., Hwang, C.Y., Kim, Y.K., Lee, Y.S., Jeong, D.H. and Cho, M.H., 2007. Antimicrobial effects of silver nanoparticles. Nanomed. Nanotechnol. Biol. Med., 3: 95–101. https://doi.org/10.1016/j.nano.2006.12.001

Mazraeh, M., Yeganeh, F.E., Youse, M., Baniyaghoob, S., Far, B.F., Akbarzadeh, I., Bigham, A., Ashra, M., Rabiee, N. and Makvandi, P., 2022. Multifunctional tetracycline-loaded silica-coated core – shell magnetic nanoparticles: Antibacterial, antibio film, and cytotoxic activities. ACS Appl. Bio Mater., 5: 1731–1743. https://doi.org/10.1021/acsabm.2c00100

Mouton, J.W., 1999. Combination therapy as a tool to prevent emergence of bacterial resistance. Infection, 27: 24–28. https://doi.org/10.1007/BF02561666

Murei, A., Ayinde, W.B., Gitari, M.W. and Samie, A., 2020. Functionalization and antimicrobial evaluation of ampicillin, penicillin and vancomycin with *Pyrenacantha grandiflora* Baill and silver nanoparticles. Sci. Rep., 10: 1–14.

https://doi.org/10.1038/s41598-020-68290-x

Nikaido, H., 2003. Molecular basis of bacterial outer membrane permeability revisited. Microbiol. Mol. Biol. Rev., 67: 593–656. https://doi.org/10.1128/MMBR.67.4.593-656.2003

Nikolova, M.P. and Chavali, M.S., 2020. Metal oxide nanoparticles as biomedical materials. Biomimetics, 5. https://doi.org/10.3390/biomimetics5020027

Nordmann, P., Cuzon, G. and Naas, T., 2009. The real threat of *Klebsiella pneumoniae* carbapenemase. Lancet Infect. Dis., 9: 228–236. https://doi.org/10.1016/S1473-3099(09)70054-4

Oueslati, M.H., Ben Tahar, L., Alzahrani, A.K. and Basha, J., 2024. Natural chalcone dye-functionalized magnetite nanoparticles: Synthesis, characterizations and performance for the removal of methylene blue and the antibacterial activity. Desalin. Water Treat., 317: 100256. https://doi.org/10.1016/j.dwt.2024.100256

Parvin, N., Joo, S.W. and Mandal, T.K., 2025. Nanomaterial-based strategies to combat antibiotic resistance: Mechanisms and applications. Antibiotics, 14: 207. https://doi.org/10.3390/antibiotics14020207

Petcharoen, K. and Sirivat, A., 2012. Synthesis and characterization of magnetite nanoparticles via the chemical co-precipitation method. Mater. Sci. Eng. B, 177: 421–427. https://doi.org/10.1016/j.mseb.2012.01.003

Raghunath, A. and Perumal, E., 2017. Metal oxide nanoparticles as antimicrobial agents: A promise for the future. Int. J. Antimicrob. Agents, 49: 137–152. https://doi.org/10.1016/j.ijantimicag.2016.11.011

Rashid, M., Rabbi, M.A., Ara, T., Hossain, M.M., Islam, M.S., Elaissari, A., Ahmad, H. and Rahman, M.M., 2021. Vancomycin conjugated iron oxide nanoparticles for magnetic targeting and efficient capture of Gram-positive and Gram-negative bacteria. RSC Adv., 11: 36319–36328. https://doi.org/10.1039/D1RA04390K

Sahoo, S., Chakraborti, C.K., Mishra, S.C., Nanda, U.N. and Naik, S., 2011. FTIR and XRD investigations of some fluoroquinolones. Int. J. Pharm. Pharm. Sci., 3: 165–170.

Saqib, S., Munis, M.F.H., Zaman, W., Ullah, F., Shah, S.N., Ayaz, A., Farooq, M. and Bahadur, S., 2018. Synthesis , characterization and use of iron oxide nano particles for antibacterial activity. Wiley Microsc. Res. Tech., pp. 1–6. https://doi.org/10.1002/jemt.23182

Sharaf, E.M., Hassan, A., AL-Salmi, F.A., Albalwe, F.M., Albalawi, H.M.R., Darwish, D.B. and Fayad, E., 2022. Synergistic antibacterial activity of compact silver / magnetite core-shell nanoparticles core shell against Gram-negative foodborne pathogens. Front. Microbiol., 13: 1–12. https://doi.org/10.3389/fmicb.2022.929491

Sharma, D., Gautam, S., Singh, S., Srivastava, N., Khan, A.M. and Bisht, D., 2025. Unveiling the nanoworld of antimicrobial resistance : Integrating nature and nanotechnology. Front. Microbiol., 15. https://doi.org/10.3389/fmicb.2024.1391345

Shi, H., Magaye, R., Castranova, V. and Zhao, J., 2013. Titanium dioxide nanoparticles: A review of current toxicological data. Part. Fibre Toxicol., 10: 1–33.

Shoudho, K.N., Uddin, S., Rumon, M.M.H. and Shakil, M.S., 2024. Influence of physicochemical properties of iron oxide nanoparticles on their antibacterial activity. ACS Omega, 9: 33303–33334. https://doi.org/10.1021/acsomega.4c02822

Soto, K., Garza, K.M. and Murr, L.E., 2007. Cytotoxic effects of aggregated nanomaterials. Acta Biomater., 3: 351–358. https://doi.org/10.1016/j.actbio.2006.11.004

Sterren, V.B., Aiassa, V., Garnero, C., Linck, Y.G., Chattah, A.K., Monti, G.A., Longhi, M.R. and Zoppi, A., 2017. Preparation of chloramphenicol/ amino acid combinations exhibiting enhanced dissolution rates and reduced drug-induced oxidative stress. AAPS Pharm. Sci. Tech., 18: 2910–2918. https://doi.org/10.1208/s12249-017-0775-4

Theodorakis, N., Feretzakis, G., Hitas, C., Kreouzi, M., Kalantzi, S., Spyridaki, A., Boufeas, I.Z., Sakagianni, A., Paxinou, E., Verykios, V.S. and Nikolaou, M., 2024. Antibiotic resistance in the elderly: Mechanisms, risk factors, and solutions. Microorganisms, 12. https://doi.org/10.3390/microorganisms12101978

Tran, N., Mir, A., Mallik, D., Sinha, A., Nayar, S. and Webster, T.J., 2010. Bactericidal effect of iron oxide nanoparticles on *Staphylococcus aureus*. Int. J. Nanomed., 5: 277–283. https://doi.org/10.2147/IJN.S9220

Tyers, M. and Wright, G.D., 2019. Drug combinations: A strategy to extend the life of antibiotics in the 21st century. Nat. Rev. Microbiol., 17: 141–155. https://doi.org/10.1038/

s41579-018-0141-x

Uddin, T.M., Chakraborty, A.J., Khusro, A., Zidan, B.R.M., Mitra, S., Emran, T. Bin, Dhama, K., Ripon, M.K.H., Gajdács, M., Sahibzada, M.U.K., Hossain, M.J. and Koirala, N., 2021. Antibiotic resistance in microbes: History, mechanisms, therapeutic strategies and future prospects. J. Infect. Publ. Health, 14: 1750–1766. https://doi.org/10.1016/j.jiph.2021.10.020

Venter, H., 2019. Reversing resistance to counter antimicrobial resistance in the World Health Organisation's critical priority of most dangerous pathogens. Biosci. Rep., 39: 1–12.

Walsh, T.R., Gales, A.C., Laxminarayan, R. and Dodd, P.C., 2023. Antimicrobial resistance: Addressing a global threat to humanity. PLoS Med., 20: 12–15. https://doi.org/10.1371/journal.pmed.1004264

Wang, N., Luo, J., Deng, F., Huang, Y. and Zhou, H., 2022. Antibiotic combination therapy: A strategy to overcome bacterial resistance to aminoglycoside antibiotics. Front. Pharmacol., 13:1–15.https://doi.org/10.3389/fphar.2022.839808

Wehbe, M., Kadah El Habbal, R., Kaj, J. and Karam, P., 2024. Synergistic dual antibacterial activity of magnetite hydrogels doped with silver. Langmuir, 40: 22865–22874. https://doi.org/10.1021/acs.langmuir.4c02964

Worthington, R.J. and Melander, C., 2013. Combination approaches to combat multidrug-resistant bacteria. Trends Biotechnol., 31: 177–184. https://doi.org/10.1016/j.tibtech.2012.12.006

Xu, C., Akakuru, O.U., Zheng, J. and Wu, A., 2019. Applications of iron oxide-based magnetic nanoparticles in the diagnosis and treatment of bacterial infections. Front. Bioeng. Biotechnol., 7: 1–15. https://doi.org/10.3389/fbioe.2019.00141

Yap, P.S.X., Lim, S.H.E., Hu, C.P. and Yiap, B.C., 2013. Combination of essential oils and antibiotics reduce antibiotic resistance in plasmid-conferred multidrug resistant bacteria. Phytomedicine, 20: 710–713. https://doi.org/10.1016/j.phymed.2013.02.013

Zhang, C., Du, C., Liao, J.-Y., Gu, Y., Gong, Y., Pei, J., Gu, H., Yin, D., Gao, L. and Pan, Y., 2019. Synthesis of Magnetite hybrid nanocomplexes to eliminate bacteria and enhance biofilm disrupting. Biomater. Sci., 7: 2833-2840. https://doi.org/10.1039/C9BM00057G

Zhang, T.G. and Miao, C.Y., 2024. Iron oxide nanoparticles as promising antibacterial agents of new generation. Nanomaterials, 14. https://doi.org/10.3390/nano14151311

Zheng, Y., Hou, L., Liu, M., Newell, S.E., Yin, G., Yu, C., Zhang, H., Li, X., Gao, D., Gao, J., Wang, R. and Liu, C., 2017. Effects of silver nanoparticles on nitrification and associated nitrous oxide production in aquatic environments. Sci. Adv., 3: 21–23. https://doi.org/10.1126/sciadv.1603229

Zhu, M., Tse, M.W., Weller, J., Chen, J. and Blainey, P.C., 2021. The future of antibiotics begins with discovering new combinations. Ann. N. Y. Acad. Sci., 1496: 82–96. https://doi.org/10.1111/nyas.14649